Assessing the Three-Dimensional Behaviour of Dry Stone Retaining Walls by Full-Scale Experiments

Hong Hanh Le, Jean Claude Morel, Anne Sophie Colas, Benjamin Terrade, Denis Garnier

ORIGINAL ARTICLE

Assessing the three-dimensional behaviour of dry stone retaining walls by full-scale experiments

Hong Hanh Le[a], Jean-Claude Morel[b], Anne-Sophie Colas[c], Benjamin Terrade[c] and Denis Garnier[d]

[a]Faculty of Building and Industrial Construction, National University of Civil Engineering, 55 Giai Phong Str. Hanoi, Vietnam; [b]School of Energy, Construction and Environment, Centre of Low Impact buildings, Faculty of Engineering, Environment & Computing, Coventry; [c]Université Paris-Est, MAST, EMGCU, IFSTTAR, 14-20 boulevard Newton, 77447 Marne-la-Vallée, France; [d] Université Paris-Est, Laboratoire Navier (UMR 8205), ENPC, IFSTTAR, CNRS, 6-8 avenue Blaise Pascal, 77455 Marne-la-Vallée, France

ARTICLE HISTORY

Compiled May 19, 2021

Abstract

Dry stone masonry is a widespread building technique, which has been used in Europe and all around the world in both monumental and vernacular architecture. Amongst them, dry stone structures retaining slopes have received growing attention over the past two decades, but only few studies concentrate on the influence of localised loading upon the backfill. This paper describes an experimental campaign, comprising two tests on full-scale structures, which has been undertaken in France in order to investigate the behaviour of dry stone road retaining walls. The results of these tests are compared with those of a previous experimental campaign, and of a theoretical approach.

KEYWORDS

Dry stone masonry; retaining walls; full-scale tests; 3D behaviour; upper-bound limit analysis

Corresponding author. Email: anne-sophie.colas@ifsttar.fr

1. Introduction

Dry stone walling is an ancient, vernacular building technique that can be found worldwide, in areas where the supply of stones is significant and planning difficult. In Europe, dry stone accounts in particular for a large part of the retaining walls along road networks. Although dry stone structures have proven their robustness and sustainability, when they experience important pathologies or collapse, they are most often replaced with concrete or gabion alternatives, because there is a lack of knowledge of this technology.

Research on dry stone masonry is mainly dedicated to building construction (Bui, Limam, Sarhosis, and Hjiaj, 2017; Lourenço, Oliveira, Roca, and Orduña, 2005; Smoljanović, Živaljić, Nikolić, and Munjiza, 2018; Walker and Dickens, 1995). Nevertheless, over the past two decades, research studies in France and in UK have been dedicated to dry stone earth retaining walls. Distinct element modelling has been developed to understand the bulging pathologies in existing walls (Claxton, Hart, McCombie, and Walker, 2005; Harkness, Powrie, Zhang, Brady, and O'Reilly, 2000; Powrie, Harkness, Zhang, and Bush, 2002; Walker, McCombie, and Claxton, 2007), based on the experimental data from (Burgoyne, 1853). On the other hand, limit equilibrium (Mundell, McCombie, Bailey, Heath, and Walker, 2009; Villemus, Morel, and Boutin, 2007), yield design (Colas, Morel, and Garnier, 2010, 2013), and distinct element (Oetomo, Vincens, Dedecker, and Morel, 2015) analyses have been performed to assess the stability of new or existing structures, calibrated and validated on dedicated full-scale tests (Colas et al., 2010; McCombie, Mundell, Heath, and Walker, 2012; Mundell, McCombie, Heath, Harkness, and Walker, 2010; Villemus et al., 2007). Numerical and theoretical developments have been exclusively performed in 2D on wall cross-sections. Only one full-scale (McCombie et al., 2012; Mundell et al., 2010) and one recent scale-down (Quezada, Vincens, Mouterde, and Morel, 2016) experimental campaign have been performed in 3D, to assess the effect of traffic on dry stone walls.

Recently, Le, Garnier, Colas, Terrade, and Morel (2016) have developed a 3D model, using yield design theory, in order to take into account the effect of axle loads on dry stone retaining structures. On-going on this study, this paper presents an experimental

campaign on full-scale point loaded retaining walls. First, the experimental configuration and protocol is detailed. The results are analysed, and compared with those of a previous experimental campaign and of a theoretical approach. Perspectives on this work include a new experimental campaign, which will be introduced in the conclusion.

2. Configuration of the experimental campaign

The experimental campaign aims at a better understanding of the three-dimensional behaviour of dry stone retaining walls. It comprises two on-site tests, undertaken in Vaucluse (France), consisting in loading until failure full-scale dry stone retaining walls with a loading plate placed on the top of the backfill (Fig. 1).

2.1. Wall construction

The experimental walls were constructed by professional dry stone wallers, following dry stone state-of-the-art practice, as detailed in (CAPEB, 2008) and included in (McCombie, Morel, and Garnier, 2015), except for through-stones, which have not been introduced in the wall in order to encourage its deformation. Nevertheless, the stones on each face overlapped and voids have been filled with small pieces of stone (Fig. 2).

The two test walls are made of limestone. They are 2.3 m high and more than 10 m long, to limit side effects during the experiment. Wall thickness has been selected based on the 2D yield design model developed by the authors (Colas et al., 2010, 2013), and on 3D full-scale experiments undertaken in the University of Bath (McCombie et al., 2012; Mundell et al., 2010). Self-standing walls are built and backfilled to the top of the wall. Walls are made of limestone, characterised by its inter-block friction angle $\phi = 36.0 \pm 0.5°$, measured by shear box testing. The backfill is made of rolled gravel. It has already been used and characterised in a previous experimental campaign (Colas et al., 2010) using triaxial test, providing an internal friction angle $\phi_s = 37.7°$. The backfill is placed without compaction, and its surface is finally levelled. The geometrical and physical characteristics of the wall, the backfill and the loading system are recorded in Table 1.

Considering this experimental campaign was the first of its kind in France, the

first experiment (wall 1) has been disrupted by several technical problems. Yet, this experiment has provided a first estimate of the ultimate load and has enabled the improvement of the experimental protocol and device. This paper will focus on the second experiment (wall 2).

2.2. Loading device and protocol

In order to simulate the action of the traffic on the retaining wall, a load was applied to the surface of the backfill via a 60×60 cm steel plate. For simplicity reasons, it has been decided to use a 34 ton excavator to apply the load (Fig. 3a). The load is measured by a load cell on which is fixed a hemi-spherical head (Fig. 3b). The load measured by the sensor is thus the vertical component of the excavator load, the horizontal component being considered as negligible, given the vertical orientation of the excavator pressure.

The loading protocol has been undertaken in 5 steps (Tab. 2). The first experiment showed that the load have no influence on the wall when applied on the surface of the backfill over 2 m from the top of the wall. This is consistent with the standard practice considering that concentrated loads irradiate with a maximal angle of 45° (EN 1991). For the second testing wall, the load was first applied at a distance $d = 1.70$ m from the top of the wall, in 2 steps. Then, the load has been moved closer, at $d = 0.50$ m from the top of the wall, and the loading process has been carried out in 3 steps. The steps are due to the steel plate, which sinks in the gravel backfill. In order to keep constant loading conditions, the loading process is stopped to remove the steel plate, add gravel and ensure a level surface of the backfill.

The wall displacements have been recorded throughout the experiment by cable sensors and at key points of the loading process using a laser measurement device.

2.3. Measurement device

2.3.1. Cable measurement device

Displacements of the wall are measured by 12 cable sensors, already used by Villemus et al. (2007) and Colas et al. (2010) in their experimental campaign. Yet, unlike the previous plane strain experimental campaigns, the sensors are disposed crosswisely, 8

on a vertical line at the middle of the wall and 5 on a horizontal line (Fig. 4), in order to measure displacements of the whole front face. They are fixed on a steel structure at one end, and on wood target stuck on blocks of the front face on the other end. The data acquisition system records the displacements every 2 seconds.

2.3.2. Laser measurement device

Along with the cable sensor system, it has been decided to use a laser measurement device to measure the wall displacements. The laser system relies on a tracker (Fig. 5a) measuring the position of 60×60 mm targets (Fig. 5b) with an accuracy of 1 mm. 20 targets are disposed on half of the front face of the wall, 5 of them being paired with cable sensor targets in order to assess the correspondence between the two measurement systems (Fig. 4). It has to be noted that laser is a one-time measurement system whereas cable system performs a continuous measurement of the wall displacements.

3. Testing results and analysis

3.1. Measurement device

This experiment provides an opportunity to test the displacement sensor device. Cable sensors have already been used by the authors for plane strain full-scale experiments and proved consistent for the measurement of the wall displacements. In this experimental campaign, it has been decided to use also laser sensors. The repartition of cable sensor and laser sensor targets are displayed in Figure 4. 10 targets (cable targets C11, C7, C2, C13, C14, and laser targets L1, L2, L3, L5, L10) have been paired in order to assess the differences between the two systems.

Figure 6 shows the displacements measured by the 5 couples of sensors for stage 1.7mII of the second experiment. This graph shows that the displacements given by the two systems have the same order of magnitude. Results are even closer for large displacements. These two systems are complementary, with the cable sensors providing continuous measurement on a limited number of targets, and the laser sensors providing a one-time measurement of a larger area.

3.2. Elasto-plastic behaviour of the structure

Figures 7 and 8 represent the load-displacement response, generated from the force measured by the force sensor, and the displacements measured by the sensors situated on the vertical axis of symmetry of the wall face (Fig. 4). Figure 7 shows the results of sensor C7, when the distance d between the load and the top of the wall equals 1.7 m, and Figure 8 shows the results of sensors C2, C4, C5, C8 and C10, for $d = 0.5$ m. The results of the other sensors were also plotted, with similar responses; they are not reported on the figures for the sake of clarity.

Considering the testing protocol (Tab. 2), which alternates loading and unloading stages of the structure, Fig. 7 shows a perfect elasto-plastic behaviour of the retaining system, comprising the wall and its backfill, during the experiment, when the load is 1.7 m distant from the wall. Figure 8 proves that the hypothesis of perfect plasticity no longer applies, when the load get closer to the top of the wall. Yet, the wall-backfill system experiences a post-peak behaviour which can be assimilated to softening.

3.3. 3D deformation of the wall

Figure 9 shows the displacement of the front face in the central cross-section of the wall, during the whole experiment. It can be noticed that, when the localised loading is far from the wall ($d = 1.7$ m), the displacements are quite small, even if the load reaches 90 kN. Displacements are much larger when the load is close to the wall, even for small loading. In a first approximation, the wall seems to experience two modes of deformation during the experiment:

- a translation of the upper two-thirds of the wall;
- a shearing of beds in the lower third of the wall.

Figures 10 and 11 show that the deformation of the wall is actually in 3D, with little displacements for side cross-sections and larger displacements in the central cross-section. These results have to be compared to Villemus et al. (2007) and Colas et al. (2013), where the deformation of a dry stone retaining wall solely loaded by its backfill is the same for every cross-section of the wall. The experimental campaign presented hereby confirms the 3D behaviour of a retaining wall subjected to a localised loading

Figure 12 shows the wall condition after failure. This confirms the 3D behaviour of the wall, as the breach is included in a 4×1.5 m rectangle located in the central part of the wall. The ends of the wall have not experienced any deformation. These observations confirm the possibility of repairing dry stone breaches with a careful reconstruction of the collapsed part of the wall.

4. Comparative analysis and discussion

4.1. Comparison with 3D full-scale testing at the University of Bath

Only two full-scale experimental campaigns have been performed in order to assess the 3D behaviour of dry stone retaining walls. The first one took place at the University of Bath (UK), comprising 5 tests on 2.5 m high walls (McCombie et al., 2012; Mundell et al., 2010). Walls were built in limestone or slate, backfilled with crushed gravel, and loaded with a hydraulic jack applied on a plate placed on the surface of the backfill. The characteristics of the walls and the tests are given in Table 3.

The two experimental campaigns are quite similar, as they both consists in building dry stone walls, backfilled with a granular material, and loading them until failure with a load applied on the backfill. Yet, the experiments differs in their objectives: the tests undertook at the University of Bath aimed at a better understanding of the pathologies of existing walls, and more especially the origin of bulge deformations. Assuming that bulges are due to the settlement of the soil of foundation, the experimental walls have been built on a steel platform which could be raised, lowered or tilted in order to simulate ground motions. The first experimental wall has been subjected to raising and tilting stages, whereas the other four walls where only raised of a few centimetres. Besides, walls 2 to 5 were deliberately built with a poorer quality of construction in order to make more realistic experiments, as most of the existing walls were not been built by skilled masons.

Both experimental campaigns prove that dry stone retaining walls subjected to a load on the surface of the backfill experience 3D behaviour. Moreover, the comparative analysis shows that dry stone walls can withstand significant deformation prior failure, showing a certain ductility, even poorly constructed. This property is a valuable asset

for monitoring and maintenance of existing walls as significant deformations provide a visual indication of the potential weakness of the structure.

4.2. Comparison with a 3D yield design model

The results of the experimental campaign have also been used to test yield design models. Comparisons have been drawn at two key-stages of the experiment: when the localised loading is placed at 1.70 m of the top of wall (stage 1.7mII), and at 0.50 m (stage 0.5mI).

For stage 0.5mI, comparisons have been performed with a 3D model developed by Le et al. (2016) to assess dry stone road retaining structures. In this model, the effects of traffic loadings have been represented by a single pointed load applied on a rigid plate on the backfill, figuring the action of an axle (Fig. 13). The model is based on the knowledge of the geometry of the structure, the loading mode and the strength criterion of the constituent materials. The 3D strength criterion of dry stone is obtained using periodic homogenisation in the framework of yield design. The strength domain of the homogenised masonry is given by:

$$G^{\text{hom}} = \left\{ \underline{\underline{\Sigma}} / \underline{\underline{\Sigma}} : \underline{\underline{D}} \leq \pi^{\text{hom}}(\underline{\underline{D}}) = \frac{C}{\tan\phi} \text{tr}(\underline{\underline{D}}) \right\} \tag{1}$$

where :

- $\underline{\underline{\Sigma}}$ is the macroscopic stress field;
- $\underline{\underline{D}}$ is the macroscopic strain rate field;
- $\pi^{\text{hom}}(\underline{\underline{D}})$ is the support function of G^{hom} depending on the cohesion C, the friction angle ϕ of the joints, and conditions on the relevant velocity fields, exposed in Le et al. (2016).

Then, yield design upper-bound approach is undertaken to assess the stability of the whole structure, comprising the dry stone wall, the backfill, and the load upon the backfill. The virtual failure mechanism families explored in this model is defined on a half-system (Fig. 13), and comprises:

- a translation $\underline{v} = v \cos\theta \, \underline{e}_1 + v \sin\theta \, \underline{e}_3$ of a polyhedron $JRSTMOPN$ of wall;

- a translation $\underline{v}_s = v_s \cos(\psi_s - \phi_s)\,\underline{e}_1 - v_s \sin(\psi_s - \phi_s)\,\underline{e}_3$ of a polyhedron $MOIKRJ$ of soil.

The kinematic approach of yield design is based on the application of the principle of virtual works and states that the work of the external forces W_e has to remain lower than the maximal resisting work W^{mr}:

$$\forall\, \underline{v} \text{ kinematically admissible, } W^{\mathrm{e}} \leq W^{\mathrm{mr}} \tag{2}$$

Considering there is no cohesion in the dry stone wall joints and within the gravel backfill, the maximum resisting work vanishes to 0. The work of the external forces is given by the sum of the work of the body forces in the wall and the backfill, and the work of the point load, so that:

$$W_e = \underbrace{\int_V \underline{\gamma}.\underline{v}\,\mathrm{d}V}_{W^e_{\mathrm{wall}}} + \underbrace{\int_V \underline{\gamma}_s.\underline{v}_s\,\mathrm{d}V}_{W^e_{\mathrm{soil}}} + \underline{F}.\underline{v}_F \tag{3}$$

The inequality exposed in (2) finally provides an upper-bound estimation of the ultimate load F^+ that the retaining system can bear :

$$F^+_{\mathrm{system}} = \min_{\substack{\mathrm{kinematic}\\ \mathrm{parameters}}} \left\{ -\frac{W^e_{\mathrm{wall}} + W^e_{\mathrm{soil}}}{v_s \sin(\psi_s - \phi_s)} \right\} \tag{4}$$

Using parameters of Tab. 1, the ultimate load is $F^+ = 189$ kN.

For stage 1.7mII, the experiment proved that the results can merely be considered as the test of the bearing capacities of the backfill soil (Fig. 14), as the wall has experienced very small displacements. It has thus been decided to use a 3D yield design model of a semi-infinite soil loaded by a localised loading (Garnier, 1995; Maghous and Garnier, 1995).

The virtual failure mechanism family is a presented at Fig. 14 for a quarter-system, given the double-symmetry of the problem:

- the volume $AA'B'BCC'$ is given a translation $\underline{v}_{s1}$;

- the volumes $AA'C'CDD'$ and $ABCK$ are given a deformation $\underline{v}_{s2} = v_{s2}\mathrm{e}^{\theta \tan\phi}\underline{e}_\theta$ and $\underline{v}_{s20}$, respectively;
- the volumes $AA'D'DEE'$ and $ABKG$ are given a translation $\underline{v}_{s3}$ and $\underline{v}_{s30}$, respectively.

The maximum resisting work W^{mr} still equals 0. The work of the external forces is given by the work due to the soil unit weight and that due to the point load, so that:

$$W_e = \underbrace{\int_V \underline{\gamma}_s.\underline{v}_s \,\mathrm{d}V}_{W^e_{\text{soil}}} + \underline{F}.\underline{v}_F \tag{5}$$

The yield design upper-bound approach (2) finally provides an estimation of the ultimate load F^+ the soil can bear:

$$F^+_{\text{soil}} = \min_{\substack{\text{kinematic}\\ \text{parameters}}} \left\{ -\frac{W^e_{\text{soil}}}{v_{s1}} \right\} \tag{6}$$

For the rounded gravel used in the experiment, the model provides an ultimate load of $F^+ = 339$ kN.

These results show that the model happens to overestimate the experimental results with a factor of 3. This can be accounted by the upper-bound nature of the theoretical approach chosen, which necessarily overestimates the actual solution, and the complexity of the 3D homogenisation and calculation processes, which prevents from computing the optimal solution.

The difference can also be due to the experimental protocol. Actually, this experimental wall does not conform to the whole standards of dry stone construction, and have intentionally been built with weaknesses. Furthermore, the vertical direction of the load upon the backfill has proven difficult to control during the test, as the steel plate sink into the gravel, despite of the use of a hemi-spherical head. This can lead to an underestimation of the load which has been really applied on the plate.

To go further in this comparison, it has been decided to introduce a reduction coefficient of the backfill soil bearing capacities, defined as the ratio between the ultimate bearing capacities of the retaining system and those of the backfill soil, considered as

a semi-infinite medium:

$$r = \frac{F^{+}_{\text{system}}}{F^{+}_{\text{soil}}} \tag{7}$$

The theoretical reduction coefficient is given by the the ratio between the ultimate loads given by equations (4) and (6). The experimental reduction coefficient is defined as the ratio between the ultimate load at stage 0.5mI (with the concentrated load at 0.5 m of the top of the wall) and that of stage 1.7mII (with the concentrated load at 1.7 m of the wall). The results are given in Tab. 4. It can be seen that the experimental and theoretical reduction coefficient are similar. This would tend to support the hypothesis of an overestimation of the 3D yield design modelling. More experimental data are needed to confirm this result.

5. Conclusions

dry stone masonry is widespread in Europe and all around the world, where it is mainly used to build road retaining walls. These earth retaining structures have received growing attention over the past two decades, to better understand their behaviour, but only few studies concentrate on the influence of localised loading on the backfill.

This paper describes an experimental campaign, which has been undertaken in France in order to investigate the behaviour of dry stone road retaining walls. Two experimental dry stone retaining walls have been built and localised loading has been applied to the surface of the backfill until failure. Tests have proven the three-dimensional behaviour of dry stone walls subjected to an axle load. Walls have experienced a deformation located around the point of load application, leading to the collapse of the central part of the wall. Comparisons with a yield design model shows a gap between theoretical and experimental results, which can be accounted for by the differences between the experimental protocol and the modelling hypotheses.

Perspectives on this work include a new experimental campaign, with different materials and geometry, complying with the modelling hypotheses. Besides, the model will also be enhanced, using numerical developments of the yield design approach exposed

here, and thus enabling the test of all the kinematically admissible virtual velocity fields. These parallel developments can lead to go further in the analysis of dry stone retaining structures, and propose a practical calculation tool dedicated to these structures.

Acknowledgements

This work is part of the French national project PEDRA 10 MGC S 017 devoted to the study of dry stone constructions. The authors would like to acknowledge the French Ministry for the Ecological and Inclusive Transition (MTES) for its financial support to this project.

Our thanks are due to Erwan Hamard, Joachim Blanc-Gonnet, Stéphane Cointet and Van Huong Tran for their technical support during the tests.

References

T.T. Bui, A. Limam, V. Sarhosis, and M. Hjiaj. Discrete element modelling of the in-plane and out-of-plane behaviour of dry-joint masonry wall constructions. *Engineering Structures*, 136:277–294, 2017.

J. Burgoyne. Revetments or retaining walls. *Corps of Royal Engineering Papers*, 3:154–159, 1853.

CAPEB. *Guide des bonnes pratiques de construction de murs de soutènement en pierre sèche*. ENTPE, Vaulx-en-Velin, 2008.

M. Claxton, R.A. Hart, P.F. McCombie, and P.J. Walker. Rigid block distinct-element modelling of dry-stone retaining walls in plane strain. *Journal of Geotechnical and Geoenvironmental Engineering*, 131(3):381–389, 2005.

A. S. Colas, J. C. Morel, and D. Garnier. Full-scale fields to assess dry-stone retaining wall stability. *Engineering Structures*, 32:1215–1222, 2010.

A. S. Colas, J. C. Morel, and D. Garnier. Assessing the two-dimensional behaviour of drystone retaining walls by full-scale experiments and yield design simulation. *Géotechnique*, 63(2): 107–117, 2013.

D. Garnier. *Analyse par la théorie du calcul à la rupture des facteurs de réduction de la capacité portante de fondations superficielles*. PhD thesis, ENPC, 1995.

R. M. Harkness, W. Powrie, X. Zhang, K. Brady, and M. O'Reilly. Numerical modelling of full-scale tests on drystone masonry retaining wall. *Géotechnique*, 50(2):165–179, 2000.

H. H. Le, D. Garnier, A-S. Colas, B. Terrade, and J-C. Morel. 3D homogenised strength criterion for masonry: application to drystone retaining walls. *Journal of the mechanics and physics of solids*, 95:239–253, 2016.

P.B. Lourenço, D.V. Oliveira, P. Roca, and A. Orduña. Dry joint stone masonry walls subjected to in-plane combined loading. *Journal of Structural Engineering*, 131(11):1665–1673, 2005.

S. Maghous and D. Garnier. Feasibility of a numerical method for computing the ultimate loads of three dimensional structures. *Mechanics Research Communications*, 22(3):279–288, 1995.

P. McCombie, C. Mundell, A. Heath, and P. Walker. Drystone retaining walls: ductile engineering structures with tensile strength. *Engineering Structures*, 45:238–243, 2012.

P. F. McCombie, J-C. Morel, and D. Garnier. *Drystone Retaining Walls: Design, Construction and Assessment*. CRC Press, London, 2015.

C. Mundell, P. McCombie, C. Bailey, A. Heath, and P. Walker. Limit-equilibrium assesement of drystone retaining structures. *Geotechnical Engineering*, 162(4):203–212, 2009.

C. Mundell, P. McCombie, A. Heath, J. Harkness, and P. Walker. Behaviour of drystone retaining structures. *Structures and Buildings*, 163 (1):3–12, 2010.

J. J. Oetomo, E. Vincens, F. Dedecker, and J-C. Morel. Modeling the 2D behavior of dry-stone retaining walls by a fully discrete element method. *International Journal for Numerical and Analytical Methods in Geomechanics*, 40(7):1099–1120, 2015.

W. Powrie, R. Harkness, X. Zhang, and D. I. Bush. Deformation and failure modes of drystone retaining walls. *Géotechnique*, 52(6):435–446, 2002.

J-C. Quezada, E. Vincens, R. Mouterde, and J-C. Morel. 3D failure of a scale-down dry stone retaining wall: a DEM modeling. *Engineering Structures*, 117:506–517, 2016.

H. Smoljanović, N. Živaljić, Ž. Nikolić, and A. Munjiza. Numerical analysis of 3D dry-stone masonry structures by combined finite-discrete element method. *International Journal of Solids and Structures*, 136-137:150–167, 2018.

B. Villemus, J. C. Morel, and C. Boutin. Experimental assessment of dry stone retaining wall stability on a rigid foundation. *Engineering Structures*, 29(9):2124–2132, 2007.

P. Walker, P. McCombie, and M. Claxton. Plane strain numerical model for drystone retaining walls. *Geotechnical Engineering*, 160(2):97–103, 2007.

P.J. Walker and J. Dickens. Stability of medieval dry stone walls in zimbabwe. *Géotechnique*,

356 45:141–147, 1995.

Figure 1. Overview of the experimental site in Vaucluse (Photo credit: J. Blanc-Gonnet).

(a) (b)

Figure 2. Testing wall 2 : elevation (a) and top view (b).

Figure 3. Experimental loading system: 34 tonne excavator (a) acting on a hemi-spherical head linked to the force sensor (b).

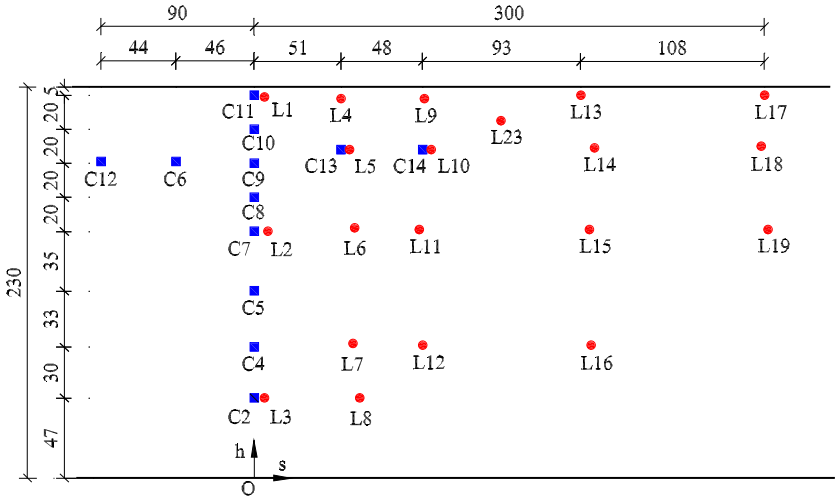

Figure 4. Distribution of the sensor targets: Ci - cable sensor target; Li - laser target (distances in cm).

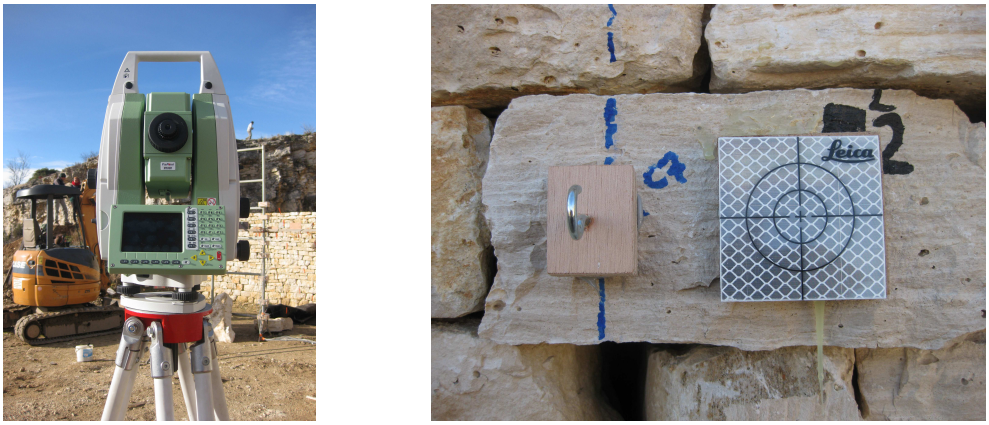

(a) (b)

Figure 5. Laser measurement device : tracker (a) and 60 × 60 mm target (b).

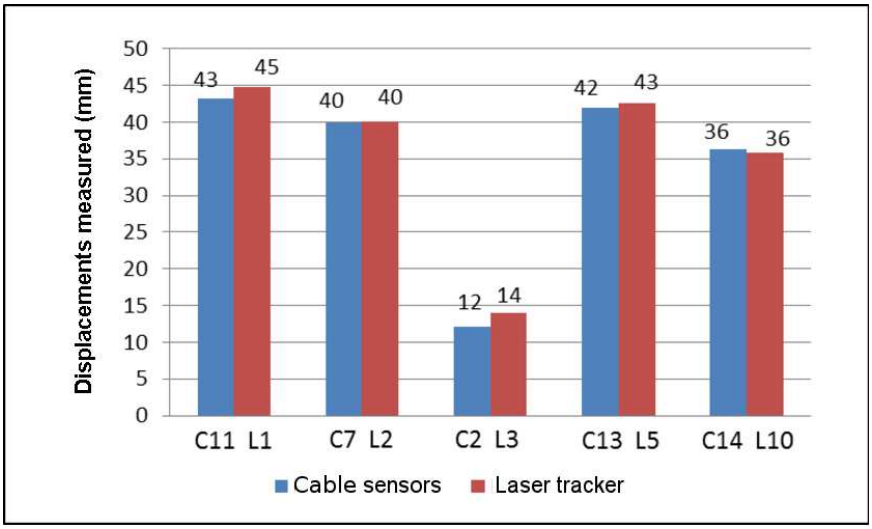

Figure 6. Comparison between the displacements measured by cable sensors and laser sensors for stage 1.7mII.

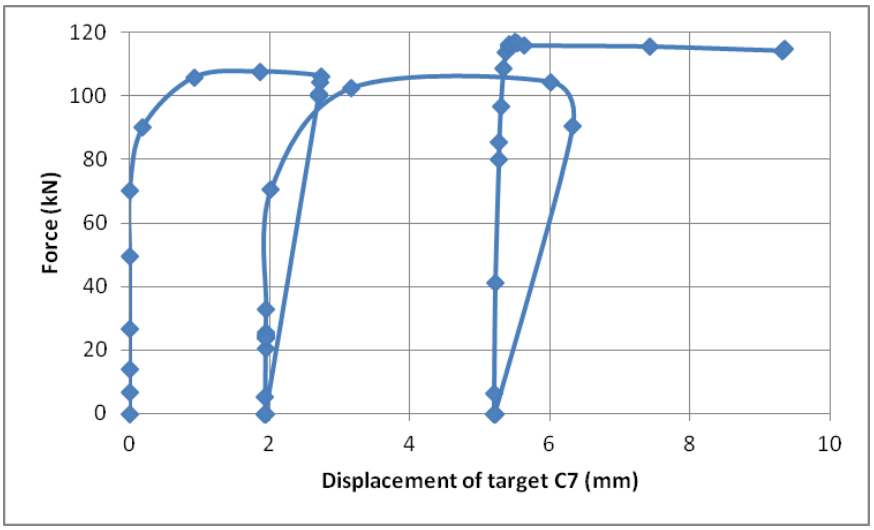

Figure 7. Force against sensor C7 displacements during stage 1.7II.

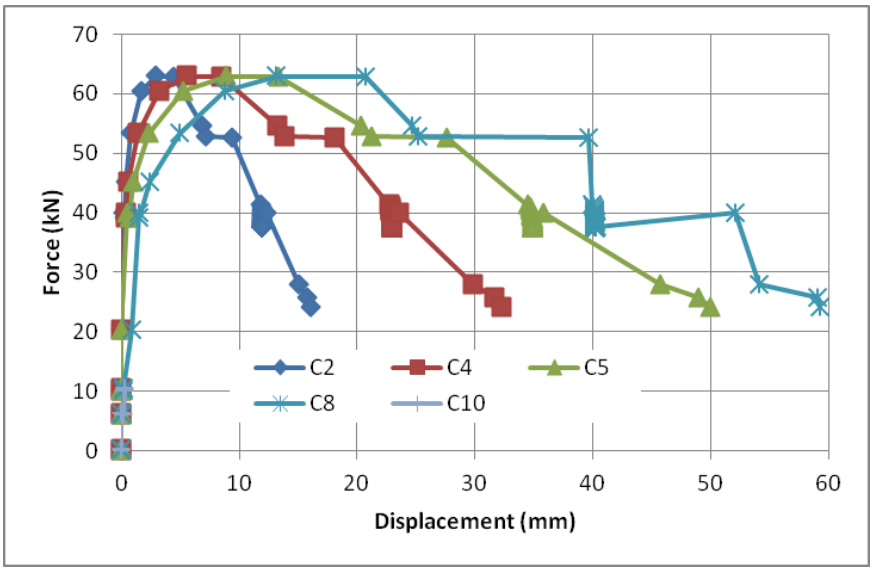

Figure 8. Force against sensors C2, C4, C5, C8 and C10 displacements during stage 0.5I.

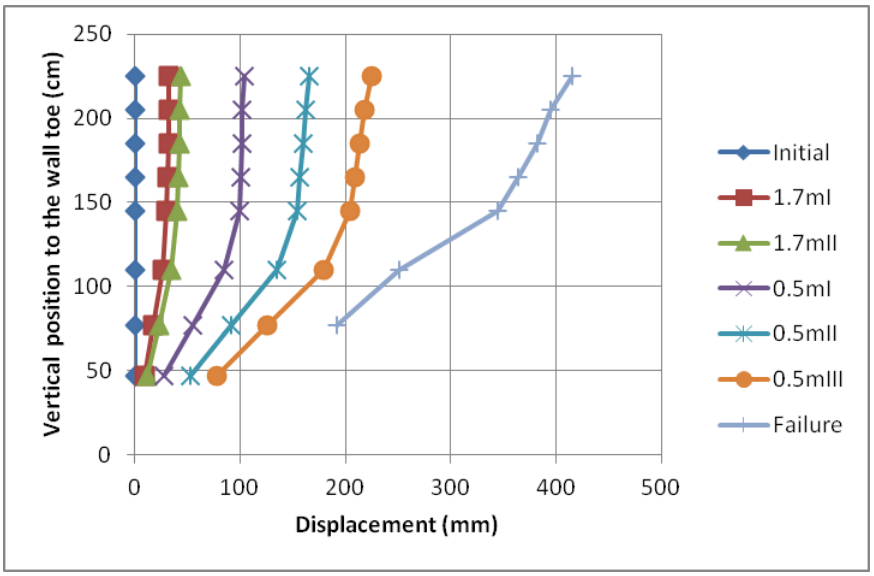

Figure 9. Evolution of the vertical axis of symmetry of the wall facing during the tests: results from sensors C2, C4, C5, C7, C8, C9, C10, C11.

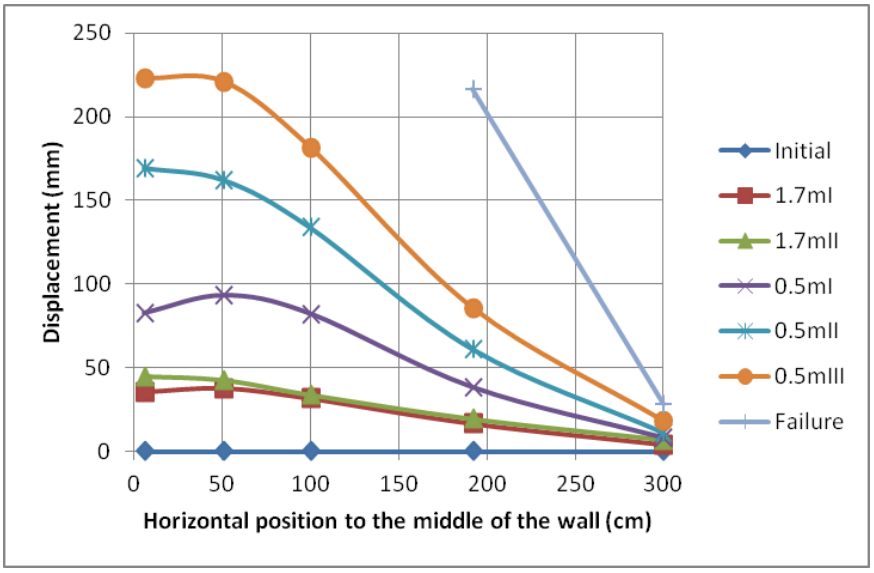

Figure 10. Evolution of a horizontal line of the wall facing during the tests: results from sensors C11, L4, L9, L13, L17

Figure 11. Deformation of the wall after stage 0.5III: top view.

Figure 12. Test wall 2 after collapse.

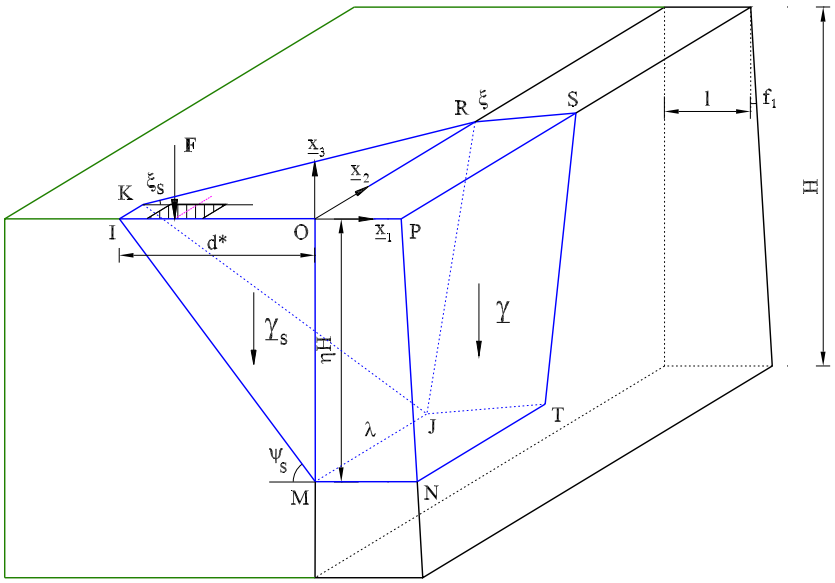

Figure 13. Half-system cross-section definition for 3D yield design analysis of the retaining wall by Le *et al.* (Le et al., 2016).

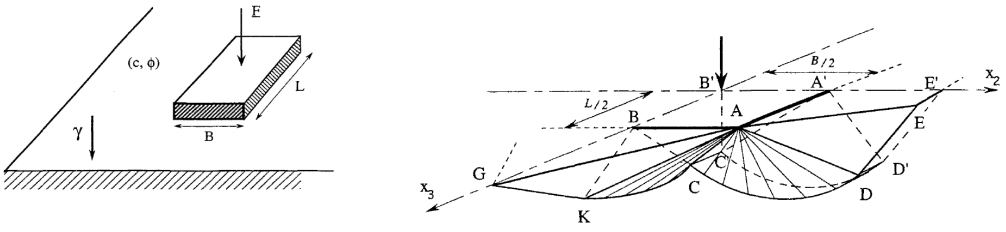

Figure 14. Test of a semi-infinite soil bearing capacities (left) and quarter-system cross-section definition for 3D yield design analysis (right).

Table 1. Experimental tests in Vaucluse: geometrical and physical characteristics, and experimental results.

	Wall 1	Wall 2
Type of stone	Limestone	Limestone
Wall height (m)	2.3	2.3
Backfill height(m)	2.3	2.3
Wall top thickness (m)	0.55	0.52
Wall length (m)	10.55	10.55
Wall batter (%)	6	6
Wall unit weight (kN/m^3)	20.3	20.3
Backfill unit weight (kN/m^3)	14.9	15.4
Block friction angle (°)	36	36
Backfill friction angle (°)	37.7	37.7
Distance load/wall (m)	0.5	0.5
Experimental load (kN)	55	63

Table 2. Testing protocol on wall 2.

Stage	Distance (m)	Maximum (kN)	Comments
1.7mI	1.70	90	Unloading, backfill levelling
1.7mII	1.70	117(143)*	Unloading
0.5mI	0.50	63	Pause
0.5mII	0.50	43	Pause
0.5mIII	0.50	37	Unloading, backfill levelling
Failure	0.50	35	Loading until failure

*117 kN: ultimate loading causing large displacements;
143 kN: maximum loading measured by the force sensor.

Table 3. Experimental tests at the University of Bath: geometrical and physical characteristics, and experimental results.

	Wall 1	Wall 2	Wall 3	Wall 4	Wall 5
Type of stone	limestone	limestone	limestone	limestone	slate
Wall height (m)	2.5	2.5	2.5	2.5	2.5
Backfill height(m)	2.2	2.2	2.2	2.2	2.2
Wall top thickness (m)	0.4	0.3	0.4	0.4	0.4
Wall batter (%)	8	8	8	12	11
Wall unit weight (kN/m^3)	19.2	19.9	16.8	17	19.7
Backfill unit weight (kN/m^3)	16.1	13.7	13.7	13.7	13.7
Block friction angle (°)	37.4	37.4	37.4	37.4	17.5
Backfill friction angle (°)	51	39	39	39	39
Distance load/wall (m)	1	1	1	1	1
Experimental load (kN)	110	75	80	85	60

Table 4. Comparison between experimental and theoretical reduction coefficient of the backfill soil bearing capacities, defined as the ratio between the ultimate bearing capacities of the retaining system F^+_{system} and those of the soil F^+_{soil}.

	Experiment	Yield design
Reduction coefficient r	0.57	0.56